JOURNAL OF MOLECULAR SPECTROSCOPY 171, 210–222 (1995)

High-Resolution Laser Excitation Spectroscopy of the $A^1\Sigma^+-X^1\Sigma^+$ Transition of BaS

ZULFIKAR MORBI AND PETER F. BERNATH[1]

Centre for Molecular Beams and Laser Chemistry, Department of Chemistry, University of Waterloo, Waterloo, Ontario, Canada N2L3G1

The high-resolution laser excitation spectrum of the $A^1\Sigma^+-X^1\Sigma^+$ transition of BaS was recorded. The BaS molecule was prepared by a gas-phase reaction of Ba metal vapor with CS_2 in a Broida oven. The 2–0, 3–0, 4–0, 5–0, 5–1, 6–1, 7–1, 7–2, 8–2, 9–2, and 8–3 vibrational bands were rotationally analyzed. Approximately 600 lines for the main isotopomer $^{138}Ba^{32}S$ (67.5%) were measured and fitted to yield spectroscopic constants for the $A^1\Sigma^+$ and $X^1\Sigma^+$ states. The $A^1\Sigma^+$ state is found to be extensively perturbed by two low-lying electronic states, the $A'^1\Pi$ and $a^3\Pi_i$.

INTRODUCTION

Alkaline earth (Mg, Ca, Ba, Sr) oxides and sulfides were once considered candidates for electronic transition chemical lasers (*1–3*). Also, interest in these molecules arises from the fact that the $A^1\Sigma^+-X^1\Sigma^+$ transition is severely affected by the presence of several other low-lying ($< 15\,000$ cm^{-1}) electronic states. In fact, all of the alkaline earth monoxides (*4–7*) and sulfides (*8–12*) are known to be extensively perturbed in their low-lying excited states. This has led to the development of a systematic classification scheme to describe the perturbations observed in these molecules (*13*). The high-resolution laser excitation spectroscopy of barium sulfide (BaS) is described in this study.

The first spectroscopic measurement of BaS was carried out by Barrow *et al.* (*14*). A red-degraded absorption spectrum centered at 3860 Å was recorded, but the instrumental resolution was insufficient to obtain a rotationally resolved spectrum. From the analysis of the vibrational structure, ground and excited state vibrational intervals, term energies, and an estimate of the ground state dissociation energy were calculated. During an attempt to record the spectrum of TiS (*15*), which can be produced by heating Ti with a sulfide salt (e.g., ZnS, CaS, or BaS) in a carbon tube furnace, a red-degraded band system of BaS was discovered in the 6450–7500 Å region. This system was assigned to the $A^1\Sigma^+-X^1\Sigma^+$ transition and, subsequently, the system between 3800 and 4200 Å was assigned as the $B^1\Sigma^+-X^1\Sigma^+$ transition of BaS. The spectra of the A–X and B–X band systems were then re-recorded at a higher resolution with a 3.4-m spectrograph (*16*). A rotational analysis of the $B^1\Sigma^+-X^1\Sigma^+$ transition was completed and molecular constants for the $B^1\Sigma^+$ and $X^1\Sigma^+$ states were determined. The $A^1\Sigma^+$ constants, however, were difficult to calculate because this state showed numerous perturbations. Rough estimates of $A^1\Sigma^+$ state constants were calculated from lines believed to be from unperturbed regions of the spectrum. Since only a few

[1] Also: Department of Chemistry, University of Arizona, Tucson, AZ 85721.

0022-2852/95 $6.00

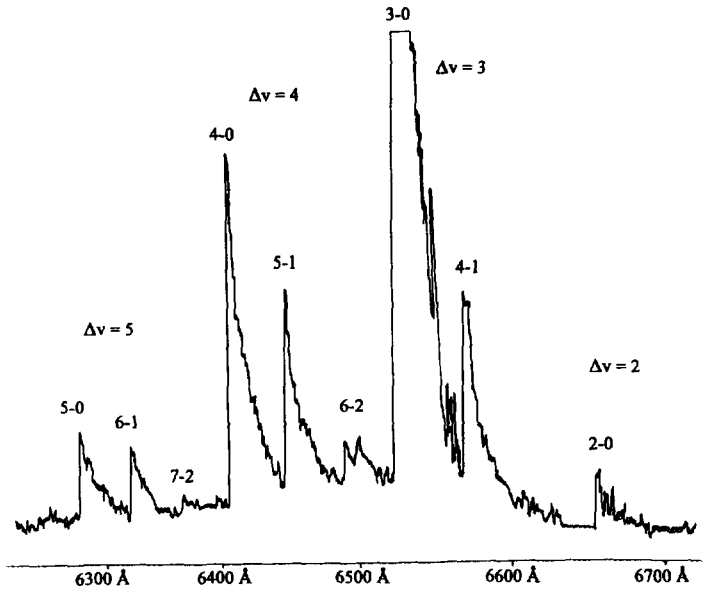

FIG. 1. Low-resolution spectrum of $A^1\Sigma^+$-$X^1\Sigma^+$ transition of BaS recorded using DCM dye.

bands (2–0, 1–0, 1–1, 0–2, 0–3) were rotationally analyzed by Barrow *et al.*, there was no attempt to derive information about the nature of the states causing the perturbations. Barrow did suggest that the observed perturbations in BaS resembled the "Y" perturbations of BaO (*13*).

The first laser spectroscopic study of BaS was completed by Cummins *et al.* (*17*). They used an argon-ion laser equipped with ultraviolet optics to excite the BaS molecule

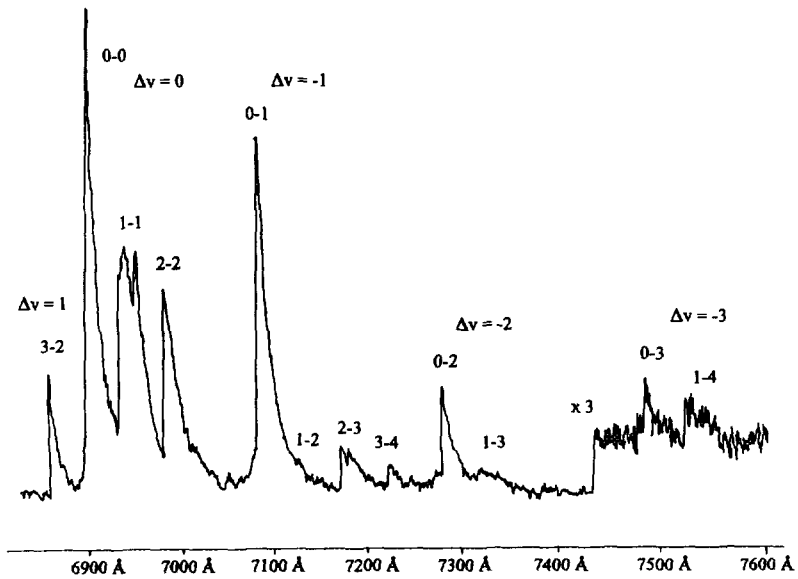

FIG. 2. Low-resolution spectrum of the $A^1\Sigma^+$-$X^1\Sigma^+$ transition of BaS recorded using pyridine 2 dye.

in a Broida oven (*20*). Three laser lines, 3336, 3551, and 3636 Å, were found to be coincident with the $B^1\Sigma^+-X^1\Sigma^+$ 12–0 $R(17)$, 6–0 $P(35)$, and 3–0 $R(125)$ rovibronic transitions of BaS. The fluorescence from the laser-excited molecules was dispersed through a monochromator and detected by a photomultiplier tube. The emission spectrum was recorded in the range 3300–9000 Å and the $B^1\Sigma^+-A'^1\Pi$, $B^1\Sigma^+-a^3\Pi_1$, and $B^1\Sigma^+-A^1\Sigma^+$ transitions were observed. A small number of lines were observed by this technique, so that it was necessary to combine these results with the data from Barrow *et al.*'s work (*16*) in order to analyze the perturbations. The $A'^1\Pi$ and $a^3\Pi_1$ states were found to lie close in energy to the $A^1\Sigma^+$ state; thus, it was possible to assign the perturbations reported by Barrow *et al.* to interactions with these states. The combination of the two data sets allowed the calculation of perturbation matrix elements, deperturbed molecular constants and potential energy curves for the low-lying electronic states of BaS (*17*). The constants derived for the $A'^1\Pi$ and $a^3\Pi_1$ states were essential for assigning the perturbations observed in the work reported here.

There have been two papers published on the pure rotational spectra of BaS. Tiemann *et al.* (*18*) vaporized 85% pure BaS at 2000 K and detected the main isotopic species of BaS (67.5% $^{138}Ba^{32}S$). Using the saturation modulation technique, they were able to measure two pure rotational transitions, ($J = 9 \leftarrow J = 8$ and $J = 11 \leftarrow J = 10$) for $v = 0, 1, 2$ of the ground state and one transition ($J = 11 \leftarrow J = 10$) for $v = 3, 4, 5$. Helms *et al.* (*19*) were able to measure 27 more pure rotational lines for the $^{138}Ba^{32}S$ (67.5%) isotopomer and also detected rotational transitions of the minor isotopes $^{137}Ba^{32}S$ (10.8%), $^{136}Ba^{32}S$ (7.4%), $^{135}Ba^{32}S$ (6.3%), $^{138}Ba^{34}S$ (3.0%), and $^{134}Ba^{32}S$ (2.3%). The BaS molecules were produced by a gas-phase reaction of Ba with OCS in an oven system based on the original Broida oven (*20*) design, as modified by Hocking *et al.* (*21*). A very accurate set of ground state rotational constants were

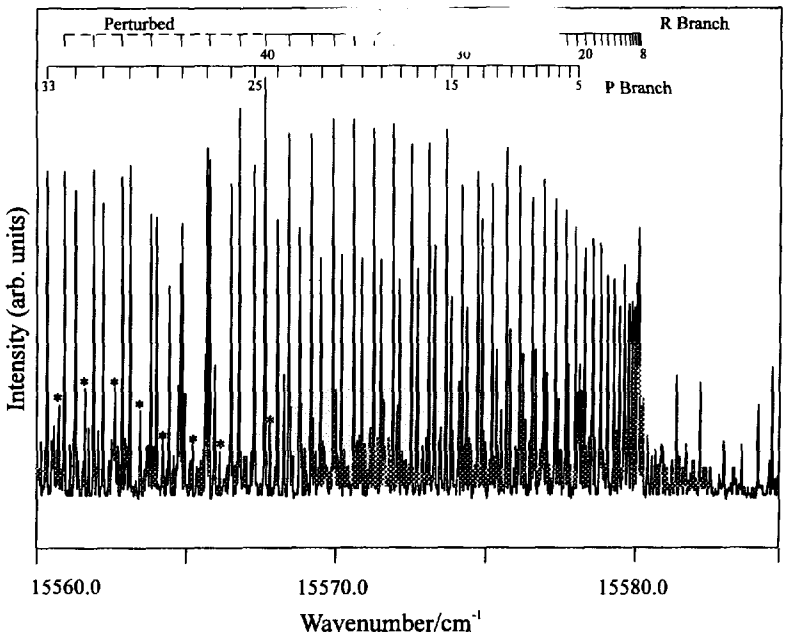

FIG. 3. High-resolution spectrum of the $A^1\Sigma^+-X^1\Sigma^+$ 4–0 band of BaS. Some lines of the 8–3 band are marked with an asterisk (*).

TABLE I

Deslandres Table for the Band Heads of the $A^1\Sigma^+$–$X^1\Sigma^+$ Transition of BaS (in cm^{-1})

v'' / v'	0		1		2		3		4
0	14459[a]	380	14079[a]	377	13703[a]	375	13328[a]		
	300		305						
1	14759[a]	375	14384[c]						13266[c]
	269								
2	15027.91[b]				14282[c]	374	13908[c]		
	275.06				274		274		
3	15302.97[b]	375	14938[c]	381	14556[c]	374	14182[c]	373	13809[c]
	277.34		276		275		275		
4	15580.31[b]	367	15213[c]	382	14832[c]	374	14457[c]		
	279.66		282		286				
5	15859.97[b]	377.12	15482.85[b]	366	15117[c]				
			280.55		281				
6			15763.40[b]	366	15398[c]				
					270				
7					15667.99[b]				
					276.17				
8					15944.16[b]	375.03	15569.13[b]		
					272.95				
9					16217.11[b]				

[a] From Barrow *et al.* (16).
[b] From high-resolution measurements (this work).
[c] Band head positions from low-resolution measurements illustrated in Figs. 1 and 2.

calculated from these data, which proved to be extremely useful in assigning the perturbed lines in the optical spectrum recorded in this work.

Melendres *et al.* (*22*) performed molecular beam electric resonance experiments on BaS and measured μ^2/B values (from the second-order Stark effect) for $v = 0$, 1, 2 of the ground state. Here μ is the electric dipole moment of the molecule and B is

TABLE II

Molecular Constants for BaS

State	v	T_v /cm^{-1}	B_v /cm^{-1}	D_v /$10^8 \cdot cm^{-1}$
$X^1\Sigma^+$	0	0.0	0.103156557(48)	3.06664(12)
	1	377.62826(62)[a]	0.102840565(78)	3.07152(28)
	2	753.5054(21)	0.102523715(13)	3.07731(71)
	3	1127.6289(22)	0.102205904(31)	3.084[b]
$A^1\Sigma^+$	2	15027.17694(85)	0.0904099(35)	-27.687(266)
	3	15302.17466(72)	0.0914075(21)	-0.535(158)
	4	15579.49504(77)	0.0915959(30)	11.135(212)
	5	15859.72294(89)	0.0914506(41)	18.129(412)
	6	16140.5521(15)	0.0913672(56)	12.051(476)
	7	16421.0237(24)	0.0897763(75)	-37.816(663)
	8	16696.9728(22)	0.0901401(17)	-2.598(55)
	9	16969.8772(22)	0.0899541(23)	4.309(134)

[a] One standard deviation uncertainty in parentheses.
[b] Fixed in the fit.

TABLE III

Summary of Perturbations in the $A^1\Sigma^+$ State

$A^1\Sigma^+$	Perturbing State		Maximum Perturbed Level
v	State	v	J
2	$a^3\Pi_2$	14	44
3	$a^3\Pi_2$	15	36
4	$A'^1\Pi$	14	43
5	$A'^1\Pi$	15	33
5	$a^3\Pi_0$	16	66
6	$a^3\Pi_0$	17	41
7	$A'^1\Pi$	18	$\geq$74
8	$A'^1\Pi$	19	69
9	$A'^1\Pi$	20	54

the rotational constant. Values for μ were not calculated for $v = 1, 2$ because rotational data were unavailable to Melendres *et al.* Barrow *et al.* (*16*) later calculated the dipole moments for $v = 0, 1, 2$ and found them to be quite large in magnitude ($\sim$10.8 D) and increased with increasing vibrational quantum number. This showed that the ground state of BaS is highly ionic and resembles a molecule made up of polarizable ions, i.e., $Ba^{2+}S^{2-}$. Large dipole moments are common for the ground and excited states of the alkaline earth monoxides (*23–26*) and show that this family of molecules have very similar electronic properties.

EXPERIMENTAL DETAILS

Barium sulfide was produced by reacting Ba (99% purity) atoms with reagent grade carbon disulfide (CS_2) in a Broida oven. The Broida oven has been described in detail elsewhere (*20*); briefly, 3–5 g of Ba (1 Torr vapor pressure at $\sim$1130 K) was placed in an alumina crucible which was resistively heated by a tungsten wire basket to the vaporize the metal. The metal vapor was then entrained in an upward flow of argon carrier gas where it eventually reacted with the oxidant gas, CS_2. The reaction produced electronically excited BaS molecules and a blue/gray chemilumescent flame. The

TABLE IV

Equilibrium Molecular Parameters for BaS

	$X^1\Sigma^+$
r_e	2.50731595(22)[1] Å
ω_e	379.3828(40)[2]
$\omega_e x_e$	0.87628(96)
B_e	0.103312863(17)
$10^4 \times \alpha_e$	3.1393(35)
$10^8 \times \gamma_e$	-6.71(85)
$10^8 \times D_e$	3.063825(37)
$10^{11} \times \beta_e$	5.33(26)

[1] One standard deviation in parentheses.
[2] All values, except r_e, are quoted in cm^{-1}.

TABLE V

Pure Rotational Transitions of $^{138}Ba^{32}S$

J'	J''	Observed	Δ	J'	J''	Observed	Δ
		$v = 0$				$v = 1$	
9	8	1.85672896 [a]	3.6×10^{-7}	9	8	1.8510418 [a]	1.2×10^{-6}
11	10	2.26928160 [a]	6.2×10^{-7}	11	10	2.26232929 [a]	3.9×10^{-7}
12	11	2.47554477	-6.3×10^{-7}	15	14	3.08480365	1.4×10^{-6}
15	14	3.09428345	7.4×10^{-7}	20	19	4.11264005	3.3×10^{-7}
18	17	3.71292052	-1.4×10^{-7}	25	24	5.14010853	-4.0×10^{-8}
19	18	3.91910803	2.3×10^{-7}	30	29	6.16711635	-3.2×10^{-7}
20	19	4.12528023	-7.2×10^{-7}	31	30	6.37245364	-1.3×10^{-6}
24	23	4.94981902	2.0×10^{-8}	35	34	7.19357083	-1.1×10^{-6}
25	24	5.15591099	-2.0×10^{-7}	40	39	8.21938262	4.9×10^{-7}
30	29	6.18608127	-1.7×10^{-7}	45	44	9.24445578	5.9×10^{-7}
31	30	6.39205206	-1.3×10^{-7}			$v = 2$	
35	34	7.21569934	-3.6×10^{-7}	9	8	1.84533742 [a]	2.9×10^{-7}
36	35	7.42154911	1.0×10^{-7}	11	10	2.25535784 [a]	-5.0×10^{-8}
40	39	8.24467455	6.0×10^{-7}	20	19	4.09996368	-1.7×10^{-7}
45	44	9.27291213	-8.0×10^{-8}	25	24	5.12426263	2.1×10^{-7}
50	49	10.30032287	3.8×10^{-7}	30	29	6.1480991	-3.0×10^{-7}
55	54	11.32681243	-3.3×10^{-7}	35	34	7.17138258	1.2×10^{-7}
		$v = 3$					
11	10	2.24836570 [a]	1.0×10^{-10}				

[a] From Tiemann *et al.* (*18*); all other values from Helms *et al.* (*19*).

typical operating pressures inside the Broida oven were 1–2 mTorr of Ba atoms, 5–10 mTorr of CS_2 oxidant gas, and 1–2 Torr of Ar carrier gas.

For the low-resolution laser excitation spectra, the all-line output of a continuous wave (cw) argon ion laser (Coherent Innova 90-4) was used to pump a cw standing wave broadband dye laser (Coherent 599-01). There were two dyes used (in separate experiments): (1) DCM dye (Exciton), which lases in the range 6200–7000 Å, and (2) Pyridine 2 dye, which lases between 6900 and 7800 Å. The output power of the dye lasers was ~300–500 mW over the tuning range of the dyes. The pump power of the argon-ion laser was 5 W.

The laser beam was introduced horizontally through the oven and focused into the center of the flame. The laser excited the molecular transition, and the resulting laser-induced fluorescence was detected by a photomultiplier tube (PMT) (Hammatsu) mounted on the side of the oven. A red-pass filter (RG700 for DCM; RG780 for Pyridine 2) was placed in front of the PMT to block the scattered laser light and some of the chemiluminescence from the flame. The output beam of the dye laser was amplitude-modulated at 3 kHz by a mechanical chopper and the signal from the PMT was demodulated by a lock-in amplifier. The output of the lock-in was sent to a chart recorder, which produced a hard copy of the spectrum (Figs. 1 and 2). A monochromator was used for calibration of the laser wavelength.

For the high-resolution scans a computer-controlled cw single-mode ring dye laser (Coherent 699-29), with a linewidth of ~1 MHz (0.00003 cm^{-1}) pumped by the all-line output of an argon-ion laser (Coherent Innova 200), was used. The ring laser was operated with Kiton Red dye (Exciton) and had an output power of ~300–400 mW.

TABLE VI

Line Positions of the $A^1\Sigma^+$–$X^1\Sigma^+$ Transition of $^{138}Ba^{32}S$

Line	Observed	Δ	Line	Observed	Δ	Line	Observed	Δ
				2–0 Band				
R(35)	15018.152	-6	R(34)	15018.810	-4	R(33)	15019.447	-1
R(32)	15020.062	1	R(31)	15020.657	4	R(30)	15021.226	3
R(29)	15021.768	-3	R(28)	15022.294	-3	R(27)	15022.798	-2
R(26)	15023.278	-4	R(25)	15023.739	-2	R(24)	15024.174	-2
R(23)	15024.583	-5	R(22)	15024.973	-4	R(21)	15025.337	-5
R(20)	15025.678	-6	R(19)	15025.998	-4	R(18)	15026.291	-5
R(17)	15026.560	-6	R(16)	15026.808	-3	R(15)	15027.030	-3
R(14)	15027.225	-4	R(13)	15027.399	-2	R(12)	15027.546	-2
R(11)	15027.669	-2	R(10)	15027.768	-1	R(9)	15027.837	-5
R(8)	15027.884	-5	R(7)	15027.908	-3	P(36)	15004.170	-6
P(35)	15005.221	-2	P(34)	15006.247	0	P(33)	15007.252	1
P(32)	15008.236	3	P(31)	15009.195	2	P(30)	15010.135	4
P(29)	15011.051	4	P(28)	15011.944	4	P(27)	15012.814	4
P(26)	15013.660	2	P(25)	15014.483	1	P(24)	15015.292	8
P(23)	15016.067	6	P(22)	15016.817	1	P(21)	15017.544	-1
P(20)	15018.253	1	P(19)	15018.933	-1	P(18)	15019.593	1
P(17)	15020.226	0	P(16)	15020.834	-1	P(15)	15021.415	-4
P(14)	15021.975	-4	P(13)	15022.512	-2	P(12)	15023.023	-1
P(11)	15023.506	-3	P(10)	15023.968	-1	P(9)	15024.408	4
P(8)	15024.815	2	P(7)	15025.203	5	P(6)	15025.558	1
P(5)	15025.896	5	P(4)	15026.203	4	P(3)	15026.488	7
P(2)	15026.748	9						
				3–0 Band				
R(40)	15290.483	-4	R(38)	15291.959	-2	R(37)	15292.663	-1
R(36)	15293.341	-3	R(35)	15294.002	1	R(34)	15294.636	2
R(33)	15295.241	-5	R(32)	15295.835	2	R(31)	15296.395	-3
R(30)	15296.941	1	R(29)	15297.458	-1	R(28)	15297.959	5
R(27)	15298.425	-2	R(26)	15298.878	2	R(25)	15299.301	-1
R(24)	15299.704	-1	R(23)	15300.085	0	R(22)	15300.438	-3
R(21)	15300.770	-3	R(20)	15301.081	-2	R(19)	15301.367	-2
R(18)	15301.631	-2	R(17)	15301.873	1	R(16)	15302.087	-1
R(15)	15302.280	-2	R(14)	15302.449	-2	R(13)	15302.598	1
R(12)	15302.718	-1	R(11)	15302.815	-3	R(10)	15302.893	-1
R(9)	15302.946	0	R(8)	15302.974	-1	P(40)	15275.672	-5
P(39)	15276.789	-2	P(38)	15277.884	0	P(37)	15278.954	2
P(36)	15279.998	1	P(35)	15281.022	2	P(34)	15282.023	3

Note. Observed-calculated values are shown in column labeled Δ ($\times 10^{-3}$).

The laser beam was introduced vertically into the Broida oven and focused in the center of the chemiluminescent flame, and the resulting laser-induced fluorescence was monitored by a PMT mounted on the side of the oven. A 75/25 beamsplitter was used to allow simultaneous recording of the excitation spectrum of I_2 for absolute wavenumber calibration (*28, 29*) of the laser. The data collection procedures and scan drive was controlled by the Coherent Autoscan software on a IBM-PC compatible computer.

A portion of the high-resolution spectrum of the 4–0 band is shown in Fig. 3. The signal-to-noise (S/N) ratio is on the order of 100:1 for the most intense lines in this portion of the spectrum. This enabled the observation of the much weaker 8–3 band which overlaps the 4–0 band. The features of the 8–3 transition are not discernible in the low-resolution spectrum of Fig. 2. Approximately 1200 cm^{-1} of data, from 15 000 to 16 200 cm^{-1}, was recorded with the single-mode laser.

TABLE VI—*Continued*

Line	Observed	Δ	Line	Observed	Δ	Line	Observed	Δ
P(33)	15282.997	0	P(32)	15283.950	-1	P(31)	15284.882	2
P(30)	15285.789	0	P(29)	15286.671	-2	P(28)	15287.532	-2
P(26)	15289.183	-4	P(24)	15290.749	2	P(23)	15291.488	-4
P(22)	15292.212	-2	P(21)	15292.910	-3	P(20)	15293.581	-7
P(19)	15294.240	0	P(18)	15294.862	-6	P(17)	15295.465	-9
P(16)	15296.055	-1	P(15)	15296.614	0	P(14)	15297.147	-2
P(13)	15297.660	-1	P(12)	15298.144	-5	P(11)	15298.615	1
P(10)	15299.056	1	P(9)	15299.471	-2	P(8)	15299.868	0
P(7)	15300.239	1	P(6)	15300.589	4	P(5)	15300.910	0
P(4)	15301.208	-1	P(3)	15301.489	2	P(2)	15301.743	3
				4–0 Band				
P(38)	15555.243	-5	P(37)	15556.325	-1	P(36)	15557.379	0
P(35)	15558.411	3	P(34)	15559.415	2	P(33)	15560.396	3
P(32)	15561.352	2	P(31)	15562.285	4	P(30)	15563.192	2
P(29)	15564.075	1	P(28)	15564.936	1	P(27)	15565.773	1
P(26)	15566.586	1	P(25)	15567.371	-3	P(24)	15568.138	-1
P(23)	15568.880	-1	P(22)	15569.597	-3	P(21)	15570.292	-2
P(20)	15570.963	-2	P(19)	15571.612	0	P(18)	15572.234	-3
P(17)	15572.837	-1	P(16)	15573.412	-3	P(15)	15573.968	-2
P(14)	15574.498	-2	P(13)	15575.011	4	P(12)	15575.494	2
P(11)	15575.954	1	P(10)	15576.390	-1	P(9)	15576.807	2
P(8)	15577.196	-1	P(7)	15577.564	-1	P(6)	15577.910	-1
P(5)	15578.232	0	P(4)	15578.533	2	P(3)	15578.810	4
P(2)	15579.056	-3	R(36)	15570.703	-6	R(35)	15571.373	-1
R(34)	15572.017	0	R(33)	15572.635	2	R(32)	15573.228	2
R(31)	15573.797	2	R(30)	15574.342	2	R(29)	15574.864	4
R(28)	15575.358	2	R(27)	15575.829	0	R(26)	15576.278	1
R(25)	15576.699	-3	R(24)	15577.100	-2	R(23)	15577.478	-2
R(22)	15577.830	-2	R(21)	15578.160	-3	R(20)	15578.466	-2
R(19)	15578.749	-2	R(18)	15579.009	-1	R(17)	15579.244	-1
R(16)	15579.455	-1	R(15)	15579.646	1	R(14)	15579.808	-2
R(13)	15579.951	-1	R(12)	15580.070	0	R(11)	15580.170	5
R(10)	15580.243	6	R(9)	15580.289	4	R(8)	15580.314	3
				5–0 Band				
R(30)	15854.343	-6	R(29)	15854.886	-1	R(28)	15855.402	2
R(27)	15855.893	5	R(26)	15856.355	4	R(25)	15856.792	2
R(24)	15857.205	3	R(23)	15857.592	0	R(22)	15857.956	0
R(21)	15858.294	-2	R(20)	15858.613	2	R(19)	15858.902	-1
R(18)	15859.167	-3	R(17)	15859.411	-2	R(16)	15859.632	0
R(15)	15859.825	-2	R(14)	15859.997	-1	P(21)	15850.446	0
P(20)	15851.124	-2	P(19)	15851.779	-1	P(18)	15852.410	-3
P(17)	15853.017	-2	P(16)	15853.601	-2	P(15)	15854.162	-1
P(14)	15854.699	0	P(13)	15855.211	1	P(12)	15855.700	1
P(11)	15856.163	-1	P(10)	15856.606	1	P(9)	15857.023	1

RESULTS

The low-resolution spectra in Figs. 1 and 2 consist of sequences of bands of the A–X transition. Each band of the system has a band head degraded to the red, suggesting an increase in bond length of the excited state. The assignment of these spectra was aided by the band head positions reported by Barrow *et al.* (*16*) and by the construction of a Deslandres table (Table I). Barrow's data provided a starting point for the construction of the Deslandres table and the band heads were inserted in the proper positions of the table. The uncertainty in the measurement of the low-resolution band head positions is ± 5 cm^{-1}. The construction of the Deslandres table gave a vibronic assignment of the low-resolution spectrum.

TABLE VI—*Continued*

Line	Observed	Δ	Line	Observed	Δ	Line	Observed	Δ
P(8)	15857.417	1	P(7)	15857.789	2	P(6)	15858.135	1
P(5)	15858.462	5						
				5–1 Band				
R(30)	15477.009	-6	R(29)	15477.535	1	R(28)	15478.030	2
R(27)	15478.501	3	R(26)	15478.947	3	R(25)	15479.367	0
R(24)	15479.765	1	R(23)	15480.141	3	R(22)	15480.489	1
R(21)	15480.813	-1	R(20)	15481.113	-3	R(19)	15481.393	-2
R(18)	15481.651	1	R(17)	15481.880	-2	R(15)	15482.272	-2
R(14)	15482.434	-2	R(13)	15482.574	0	R(12)	15482.689	-1
R(11)	15482.782	0	R(10)	15482.851	0	P(32)	15464.059	-6
P(31)	15464.992	-2	P(30)	15465.902	2	P(29)	15466.782	2
P(28)	15467.640	3	P(27)	15468.473	4	P(26)	15469.279	0
P(25)	15470.064	1	P(24)	15470.823	-1	P(23)	15471.563	2
P(22)	15472.274	0	P(21)	15472.962	-1	P(20)	15473.631	1
P(19)	15474.272	-1	P(18)	15474.891	-1	P(17)	15475.486	-2
P(16)	15476.059	-2	P(15)	15476.605	-5	P(14)	15477.135	-1
P(13)	15477.640	0	P(12)	15478.121	1	P(11)	15478.578	1
P(10)	15479.012	1	P(9)	15479.422	-1	P(8)	15479.799	-11
P(7)	15480.179	3	P(6)	15480.521	3	P(5)	15480.840	2
				6–1 Band				
P(34)	15742.944	-5	P(33)	15743.924	-1	P(32)	15744.877	1
P(31)	15745.804	0	P(30)	15746.709	2	P(29)	15747.588	2
P(28)	15748.444	2	P(27)	15749.276	1	P(26)	15750.083	1
P(25)	15750.866	-1	P(24)	15751.629	0	P(23)	15752.366	0
P(22)	15753.078	-2	P(21)	15753.769	-2	P(20)	15754.437	-2
P(19)	15755.080	-3	P(18)	15755.704	1	P(17)	15756.299	-2
P(16)	15756.873	-2	P(15)	15757.424	-1	P(14)	15757.955	1
P(13)	15758.456	-2	P(12)	15758.940	0	P(11)	15759.400	2
P(10)	15759.836	2	P(9)	15760.247	1	P(8)	15760.639	4
R(31)	15757.282	-4	R(30)	15757.829	3	R(29)	15758.344	1
R(28)	15758.837	1	R(27)	15759.308	3	R(26)	15759.752	2
R(25)	15760.170	-1	R(24)	15760.570	2	R(23)	15760.942	0
R(22)	15761.293	0	R(21)	15761.618	-1	R(20)	15761.922	-1
R(19)	15762.201	-1	R(18)	15762.457	-2	R(17)	15762.690	-1
R(16)	15762.898	-3	R(15)	15763.086	-1	R(14)	15763.261	11
R(13)	15763.398	9						
				7–1 Band				
P(34)	16022.148	-5	P(33)	16023.165	-4	P(32)	16024.165	2
P(31)	16025.142	6						
				7–2 Band				
P(33)	15647.642	-5	P(32)	15648.619	-1	P(31)	15649.573	1
P(30)	15650.502	-2	P(29)	15651.418	5	P(28)	15652.306	4
P(27)	15653.172	3	P(26)	15654.012	0	P(24)	15655.634	1

Following the vibrational assignment of the low-resolution spectrum, the high-resolution spectra of the 2–0, 3–0, 4–0, 5–0, 6–0, 5–1, 6–1, 7–1, 7–2, 8–2, 9–2, and 8–3 bands were recorded. The line positions were measured using PC-DECOMP[2] which fits the line to a Voigt lineshape function. The lines were then arranged into *P* and *R* branches belonging to a single band by using an interactive color Loomis–Wood (*27*) program. This program is a very useful for arranging large amounts of spectral data into separate series of lines, but it cannot give a unique rotational assignment. The method of ground state combination differences was used to obtain an absolute ro-

[2] Developed by J. Brault, National Solar Observatory, Tucson, AZ.

TABLE VI—*Continued*

Line	Observed	Δ	Line	Observed	Δ	Line	Observed	Δ
P(23)	15656.406	-3	P(22)	15657.158	-3	P(21)	15657.887	-3
P(20)	15658.593	-3	P(19)	15659.275	-3	P(18)	15659.933	-3
P(17)	15660.567	-2	P(16)	15661.182	3	P(15)	15661.762	-1
P(14)	15662.325	1	P(13)	15662.866	7	P(12)	15663.375	6
R(27)	15663.098	2	R(26)	15663.580	6	R(25)	15664.036	5
R(24)	15664.469	4	R(23)	15664.880	2	R(22)	15665.266	0
R(21)	15665.631	-2	R(20)	15665.974	-1	R(19)	15666.292	-3
R(18)	15666.583	-8	R(17)	15666.855	-8	R(16)	15667.106	-5
R(15)	15667.333	-2	R(14)	15667.533	-1	R(13)	15667.708	-1
R(12)	15667.860	1	R(11)	15667.990	5			
				8–2 Band				
P(49)	15904.615	-8	P(48)	15905.984	-6	P(47)	15907.331	-4
P(46)	15908.657	1	P(45)	15909.956	1	P(44)	15911.231	2
P(43)	15912.484	3	P(42)	15913.711	3	P(41)	15914.917	4
P(40)	15916.097	4	P(39)	15917.253	3	P(38)	15918.384	1
P(37)	15919.493	0	P(36)	15920.579	1	P(35)	15921.640	0
P(34)	15922.675	-2	P(33)	15923.688	-3	P(32)	15924.680	-1
P(31)	15925.643	-4	P(30)	15926.585	-3	P(29)	15927.502	-4
P(28)	15928.394	-5	P(27)	15929.263	-5	P(26)	15930.114	1
P(25)	15930.929	-5	P(24)	15931.723	-7	P(23)	15932.499	-3
P(22)	15933.245	-4	P(21)	15933.967	-4	P(20)	15934.666	-4
P(19)	15935.342	-2	P(18)	15935.994	0	P(17)	15936.619	1
P(16)	15937.218	0	P(15)	15937.797	3	P(14)	15938.348	3
P(13)	15938.875	4	P(12)	15939.375	1	P(11)	15939.855	4
P(10)	15940.312	9	P(9)	15940.738	7	P(8)	15941.142	8
P(6)	15941.875	10	R(47)	15924.478	-6	R(46)	15925.439	-4
R(45)	15926.377	-3	R(44)	15927.293	0	R(43)	15928.185	3
R(42)	15929.049	1	R(41)	15929.893	3	R(40)	15930.712	3
R(39)	15931.509	4	R(38)	15932.279	3	R(37)	15933.026	2
R(36)	15933.751	2	R(35)	15934.451	2	R(34)	15935.125	0
R(33)	15935.780	1	R(32)	15936.406	0	R(31)	15937.012	1
R(30)	15937.594	2	R(29)	15938.148	0	R(28)	15938.679	-1
R(27)	15939.186	-2	R(26)	15939.670	-1	R(25)	15940.128	-3
R(24)	15940.567	0	R(23)	15940.975	-2	R(22)	15941.362	-1
R(21)	15941.723	-3	R(20)	15942.062	-1	R(19)	15942.375	-1
R(18)	15942.663	-2	R(17)	15942.928	-1	R(16)	15943.168	-1
R(15)	15943.385	1	R(14)	15943.576	2	R(13)	15943.741	1
R(12)	15943.883	2	R(11)	15943.997	0	R(10)	15944.093	4
R(9)	15944.163	7						
				9–2 Band				
P(42)	16186.086	-2	P(41)	16187.325	-1	P(40)	16188.540	0
P(39)	16189.730	3	P(38)	16190.893	3	P(37)	16192.025	-2
P(36)	16193.143	4	P(34)	16195.286	0	P(33)	16196.323	0
P(32)	16197.334	1	P(31)	16198.320	2	P(30)	16199.279	0

tational assignment of the lines in a band. An excellent set of constants for the first three vibrational levels in the ground state was reported by Helms *et al.* (*19*), which simplied the task of assigning the perturbed lines of the spectrum.

The assigned rotational lines were then tilted to the customary $^1\Sigma$ energy level expression,

$$E_{v,J} = T_v + B_v J(J+1) - D_v[J(J+1)]^2 + H_v[J(J+1)]^3 + \cdots,$$

using a weighted least-squares fitting program. To uncover any errors in assignment or badly measured lines, each band was individually fitted by fixing the ground state

TABLE VI—*Continued*

Line	Observed	Δ	Line	Observed	Δ	Line	Observed	Δ
P(29)	16200.215	1	P(28)	16201.120	-3	P(27)	16202.007	-1
P(26)	16202.868	0	P(25)	16203.701	0	P(24)	16204.511	0
P(23)	16205.291	-3	P(22)	16206.048	-5	P(21)	16206.783	-2
P(20)	16207.491	-2	P(19)	16208.178	2	P(18)	16208.835	0
P(17)	16209.465	-1	P(16)	16210.073	-1	P(15)	16210.659	3
P(14)	16211.213	0	P(13)	16211.746	0	P(12)	16212.252	0
P(11)	16212.733	0	P(9)	16213.623	2	P(7)	16214.409	1
P(6)	16214.768	4	P(5)	16215.092	-4	P(4)	16215.401	1
P(3)	16215.688	6	P(2)	16215.936	-1	R(41)	16202.229	-4
R(40)	16203.087	-2	R(39)	16203.919	1	R(38)	16204.723	0
R(37)	16205.503	1	R(36)	16206.256	1	R(35)	16206.983	0
R(34)	16207.687	1	R(33)	16208.366	3	R(32)	16209.016	0
R(31)	16209.646	4	R(30)	16210.243	-1	R(29)	16210.820	1
R(28)	16211.367	-3	R(27)	16211.896	0	R(25)	16212.871	0
R(22)	16214.143	-1	R(21)	16214.518	0	R(20)	16214.865	-2
R(19)	16215.189	-2	R(18)	16215.489	1	R(17)	16215.761	0
R(16)	16216.010	0	R(15)	16216.231	-1	R(14)	16216.429	-1
R(13)	16216.604	2	R(12)	16216.746	-3	R(11)	16216.870	-1
R(10)	16216.967	0	R(9)	16217.038	-1	R(8)	16217.086	0
R(7)	16217.109	2						
				8–3 Band				
P(34)	15548.935	2	P(33)	15549.925	1	P(32)	15550.893	-1
P(31)	15551.840	1	P(30)	15552.760	-1	P(29)	15553.659	0
P(28)	15554.530	-4	P(27)	15555.384	-1	P(26)	15556.213	0
P(25)	15557.017	1	P(24)	15557.794	-3	P(23)	15558.553	-1
P(22)	15559.288	2	P(21)	15559.992	-3	P(20)	15560.679	-1
R(38)	15558.630	6	R(37)	15559.355	7	R(36)	15560.057	8
R(35)	15560.731	5	R(34)	15561.383	3	R(33)	15562.012	1
R(32)	15562.621	2	R(30)	15563.769	5	R(29)	15564.297	-4
R(28)	15564.812	-2	R(27)	15565.305	0	R(25)	15566.216	1
R(24)	15566.637	3	R(23)	15567.028	-2	R(22)	15567.398	-3
R(21)	15567.744	-5	R(20)	15568.075	2	R(19)	15568.371	-3
R(18)	15568.647	-3	R(16)	15569.134	2			

constants to those obtained from the microwave data and allowing only the excited state constants to vary. Then a global fit to the data was performed by combining lines from the laser and microwave experiments and allowing all constants to vary. The final fit of the data gave the molecular constants reported in Table II. Note that only lines which were locally unperturbed were included in these fits. These lines are listed in Table VI. The ground state equilibrium molecular constants are shown in Table IV. Equilibrium molecular constants for the $A\,^1\Sigma^+$ state cannot be calculated due to the global perturbations.

PERTURBATIONS IN THE $A\,^1\Sigma^+$ STATE

There are extensive perturbations in the $A\,^1\Sigma^+$ state of BaS. This can be seen by inspection of Table II, in which the centrifugal distortion constant D_v and the rotational constant B_v have a very irregular dependence on v. The negative D values for $v = 3$, 4, 7, and 8 indicate that the physical significance of D_v has been lost, and thus meaningful equilibrium rotational constants could not be calculated. For the low vibrational levels, one would expect a linear Birge–Sponer plot. This plot, of the first difference $\Delta G_{v+1/2}$ vs v, for the $A\,^1\Sigma^+$ state shows an almost parabolic dependence on v (Fig. 4). This is evidence of a global for the global perturbation of the $A\,^1\Sigma^+$ state, and hence equilibrium vibrational parameters cannot reported for this state.

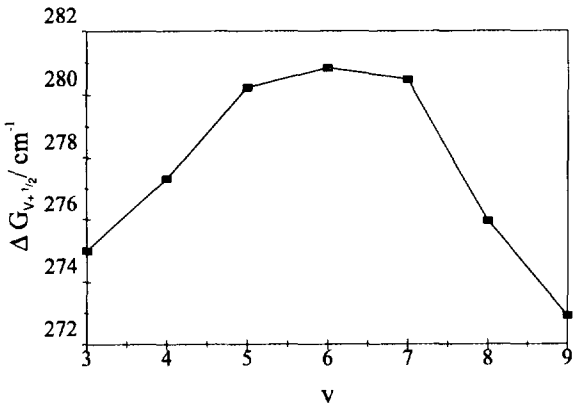

FIG. 4. Birge–Sponer plot for the $A^1\Sigma^+$ state of BaS. The nonlinearity of the plot is evidence for global perturbations in this state.

The traditional graphical procedure of using reduced term energy plots of the "perturbing states" and the $A^1\Sigma^+$ state was employed to determine the identity of the perturbing states. Molecular constants for the perturbing states obtained in the previous work by Cummins *et al.* (*17*), allowed easy identification of these states. A summary of the perturbations are listed in Table III. Since we plan to collect additional data on the infrared vibrational and near-infrared electronic transitions in the future, a deperturbation analysis was not carried out at this time.

CONCLUSIONS

The spectra recorded for this study represent an improvement in the quality of spectral data available for the $A^1\Sigma^+-X^1\Sigma^+$ transition of BaS. The previous experiments (*16, 17*) were limited by the resolution of the spectrometer and the small number of bands recorded. The resolution of the spectral lines reported here are limited by Doppler broadening in the low-pressure chemilumescent flame present in the Broida oven.

The $A^1\Sigma^+$ state was found to be extensively perturbed, with evidence of both local perturbations and global perturbations. Global perturbations are evident in $v = 3$, 4, 7, and 8 where the centrifugal distortion constants D_v are negative. In addition, perturbing energy levels have been identified and confirm the previous deperturbation analysis (*17*). There was no attempt to fit the perturbations observed in the $A^1\Sigma^+$ state at this time. There are many weak lines in the spectrum that were unassigned and are likely due to transitions from the "perturbing" states to the $X^1\Sigma^+$ state and from minor isotopomers of BaS. New experiments such as resolved fluorescence are planned, as well as direct infrared measurements in the ground state in order to improve significantly the understanding of the perturbations in the $A^1\Sigma^+$ state of BaS.

ACKNOWLEDGMENTS

This work was supported by the Natural Sciences and Engineering Research Council of Canada (NSERC). We thank Mike Dulick for his invaluable assistance in setting up the laser spectroscopy laboratory at the University of Waterloo.

RECEIVED: December 6, 1994

REFERENCES

1. D. J. Bernard, W. D. Slafer, P. J. Love, and P. H. Lee, *Appl. Opt.* **16,** 2108–2115 (1977).
2. R. W. Field, C. R. Jones, and H. P. Broida, *J. Chem. Phys.* **60,** 4377–4382 (1974).
3. D. G. Sutton and S. N. Suchard, *Appl. Opt.* **14,** 1898–1910 (1975).
4. M. Hutlin and A. Lagerqvist, *Ark. Fys.* **2,** 471–507 (1951).
5. A. Lagerqvist, E. Lind, and R. F. Barrow, *Proc. Phys. Soc. A* **63,** 1132 (1950).
6. I. Kovacs and A. Lagerqvist, *Ark. Fys.* **2,** 411–426 (1951).
7. G. Almkvist and A. Lagerqvist, *Ark. Fys.* **2,** 233–251 (1950).
8. M. Marcano and R. F. Barrow, *Trans. Faraday Soc.* **66,** 2936–2938 (1970).
9. F. S. Pianalto, Master's thesis, University of Arizona, Tucson, AZ, 1988.
10. C. J. Cheetham, W. J. M. Gissane, and R. F. Barrow, *Trans. Faraday Soc.* **61,** 1308–1316 (1965).
11. B. Pouilly, J. M. Robbe, J. Schamps, R. W. Field, and L. Young, *J. Mol. Spectrosc.* **96,** 1–55 (1982).
12. R. C. Blues and R. F. Barrow, *Trans. Faraday Soc.* **65,** 646–648 (1969).
13. R. W. Field, *J. Chem. Phys.* **60,** 2400–2413 (1974).
14. R. F. Barrow, W. J. M. Gissane, and G. V. M. Rose, *Proc. Phys. Soc.* **84,** 1035 (1964).
15. R. M. Clements and R. F. Barrow, *Chem. Commun.* **22,** 1408 (1968).
16. R. F. Barrow, W. G. Burton, and P. A. Jones, *J. Mol. Spectrosc.* **90,** 902–906 (1970).
17. P. G. Cummins, R. W. Field, and I. Renhorn, *Trans. Faraday Soc.* **90,** 327–352 (1981).
18. E. Tiemann, C. Ryzlewicz, and T. Törring, *Z. Naturforsch.* **31,** 128–130 (1976).
19. D. A. Helms, M. Winnewisser, and G. Winnewisser, *J. Phys. Chem.* **84,** 1758–1765 (1976).
20. J. B. West, R. S. Bradford, J. D. Eversole, and C. R. Jones, *Rev. Sci. Instrum.* **46,** 164–168 (1975).
21. W. H. Hocking, E. F. Pearson, R. A. Creswell, and G. Winnewisser, *J. Chem. Phys.* **68,** 1128–1134 (1978).
22. C. A. Melendres, A. J. Herbert, and K. Street, Jr., *J. Chem. Phys.* **51,** 855–856 (1969).
23. G. Dohnt, A. Hese, A. Renn, and H. S. Schweda, *Chem. Phys.* **42,** 183–190 (1979).
24. H. S. Schweda, A. Renn, H. Busener, and A. Hese, *Chem. Phys.* **98,** 157–165 (1985).
25. L. Wharton, M. Kaufman, and W. Klemperer, *J. Chem. Phys.* **37,** 621–626 (1962).
26. L. Wharton, M. Kaufman, and W. Klemperer, *J. Chem. Phys.* **43,** 943–952 (1965).
27. F. W. Loomis and R. W. Wood, *Phys. Rev.* **32,** 223–236 (1928).
28. S. Gerstenkorn and P. Luc, "Atlas du Spectre d'Absorption de la Molécule d'Iode," Laboratorie Amie-Cotton, CNRS 9145, Orsay, France, 1978.
29. S. Gerstenkorn and P. Luc, *Rev. Phys. Appl.* **14,** 791–796 (1978).